

The University of Western Australia's Resonant-bar Gravitational Wave Experiment*

M. E. Tobar, D. G. Blair, E. N. Ivanov, F. van Kann, N. P. Linthorne, P. J. Turner and I. S. Heng

Department of Physics, University of Western Australia,
Nedlands, WA 6009, Australia.

Abstract

The cryogenic resonant-mass gravitational radiation antenna at the University of Western Australia (UWA) has obtained a noise temperature of <2 mK using a zero order predictor filter. This corresponds to a 1 ms burst strain sensitivity of 7×10^{-19} . The antenna has been in continuous operation since August 1993. The antenna operates at about 5 K and consists of a 1.5 tonne niobium bar with a 710 Hz fundamental frequency, and a closely tuned secondary mass of 0.45 kg effective mass. The vibrational state of the secondary mass is continuously monitored by a 9.5 GHz superconducting parametric transducer. This paper presents the current design and operation of the detector. From a two-mode model we show how we calibrate, characterise and theoretically determine the sensitivity of our detector. Experimental results confirm the theory.

1. Introduction

Resonant-mass gravitational wave (GW) antennas have been painstakingly improved over the past 20 years (Hamilton 1992; Astone *et al.* 1993). Cryogenic operation, superconducting transducers, improved vibration isolation and increased acoustic Q -factors have contributed to a 10^4 fold improvement in energy sensitivity over Weber's (1960) original antennas. Two types of superconducting transducers have been developed: SQUID based inductive or capacitive sensors (Michelson and Taber 1981) and parametric transducers utilising radio frequency (Bocko and Johnson 1984) or microwave resonators (Veitch *et al.* 1987). Although the latter devices have been promoted as potentially very sensitive transducers, they have not previously been successfully implemented in a full scale antenna. The problems encountered included the possibility of the transducer causing parametric excitations of the antenna (Braginsky and Manukin 1977), excess noise due to the microwave readout electronics, and the effects of low frequency seismic noise.

The UWA detector consists of a niobium bending flap of 0.45 kg effective mass tuned near to the fundamental frequency of a 1.5 tonne niobium resonant bar, configured with a 9.5 GHz re-entrant cavity parametric transducer. We report the first successful operation of a large scale cryogenic resonant-mass antenna instrumented with a superconducting parametric transducer. We show that the system achieves a noise temperature of less than 2 mK, which represents a

* Refereed paper based on a contribution to the inaugural Australian General Relativity Workshop held at the Australian National University, Canberra, in September 1994.

three-fold increase in noise energy sensitivity over SQUID based systems operated to date. Parametric instability of the antenna is avoided by controlled operation in the cold damped regime where the mean energy of antenna displacement fluctuations is about 10 times less than the unloaded value. The noise in the readout electronics is reduced by using a 10 GHz sapphire loaded superconducting cavity oscillator (Giles *et al.* 1989) with the lowest ever measured phase noise at 1 kHz (Tobar and Blair 1994), and cryogenic microwave amplification employing an active carrier suppression technique (Ivanov *et al.* 1993*a*). The effect of seismic noise is greatly reduced by an improved cryogenic vibration isolation system (Blair *et al.* 1993) and a non-contacting microwave coupling to the transducer (Ivanov *et al.* 1993*b*).

A lumped-mass model of a resonant mass interacting with a capacity transducer was implemented to characterise and calculate the potential sensitivity of the UWA GW detector. The validity of the model was confirmed by showing its consistency with measured parameters and the sensitivity of the detector. A frequency domain approach is adopted here, similar to the methods used at Stanford University (Michelson and Taber 1981; Price 1987), Louisiana State University (Xu *et al.* 1989) and the University of Maryland (Richard 1986) which all use transducers based on SQUID amplifiers.

2. Cryostat

The new gravitational wave dewar design has been previously described (Blair *et al.* 1992), and is shown in Fig. 1. The thermal vacuum vessel is a stainless steel cylinder 4 m long and 1.6 m in diameter with two removable domed ends. Inside, two concentric copper shields surround the combined helium storage vessel and experimental space to shield it from room temperature radiation. The liquid nitrogen shield is suspended by fine steel cables from the vacuum vessel, and the 30 K shield hangs in a similar fashion from the liquid nitrogen shield. Both shields are constructed of copper sheet that is soft soldered to a frame of copper pipes, and both are wrapped in layers of superinsulation. Liquid nitrogen is injected into the nitrogen shield every few hours to maintain its temperature at about 120 K. Boil-off gas from the liquid helium storage shell circulates through the inner shield to make efficient use of the enthalpy remaining in the cold gas before recovery.

The experimental vessel is a double walled cylinder 3 m long, with an outer diameter of 0.96 m and an inner diameter of 0.87 m. The annular space forms the liquid helium storage shell, and has a capacity of about 380 litres. The axis of the inner cylinder is fixed below the axis of the outer cylinder to maximise the time that the internal wall is covered by liquid helium. A copper sheet framework within the liquid helium storage volume promotes convection to ensure temperature uniformity even when the liquid helium level is low.

The experimental space is supported near its centre by a 100 mm diameter thin-walled stainless steel tube which also acts as the pumping line. The experimental space forms a common vacuum space with the volume that houses the room temperature vibration isolation stack. This vacuum space is separate from that of the main dewar thermal vacuum. The niobium bar and its associated cryogenic suspension components are suspended from the top of the room temperature

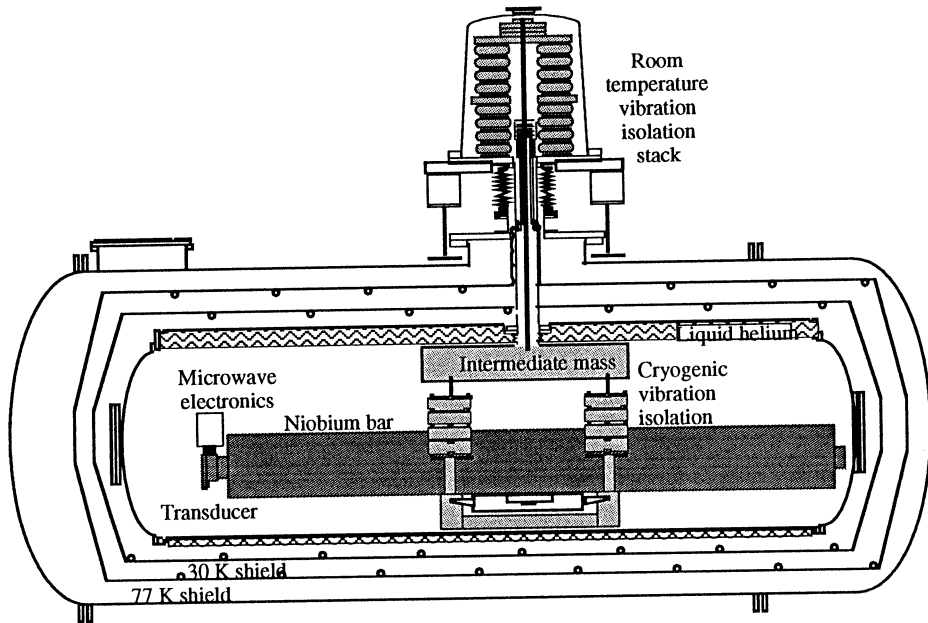


Fig. 1. Cross section of the antenna showing the niobium bar and vibration isolation system.

vibration stack by an 11.2 mm diameter titanium alloy suspension rod which hangs in the centre of the experimental space pumping tube. The niobium bar and its suspension have no mechanical contact with the surrounding cryostat except via the suspension rod at the base of the room temperature vibration isolation stack. Mechanical and acoustic noise sources within the dewar, such as boiling cryogenics and structural vibrations, are completely separated from the suspension of the niobium bar.

A key problem in the design of this suspension was in dealing with the heat flux down the suspension rod. A novel and effective solution to this problem is provided by a radiative heat shunt (Turner and Blair 1992). A set of blackened copper fins is attached to the suspension rod and interleaved with, but not contacting, a second set of fins attached to the inside of the pumping tube. The second set of fins is thermally grounded through the pumping tube to the liquid nitrogen shield. The heat shunt reduces the temperature of the suspension rod at this point from near room temperature to less than 130 K. The heat flux into the 4.2 K environment is thus reduced by a factor of about 4, to 40 mW. This excess heat flux is balanced by thermal conduction through the low pressure (10^{-4} Torr) helium exchange gas in the experimental space. At this pressure the equilibrium temperature of the antenna is about 5.7 K, the acoustic Q s of the fundamental modes of the antenna exceed 10^7 , and the antenna has a 27 dB acoustic margin from the ambient laboratory noise level (i.e. the ambient noise level has to be raised by 27 dB to effect our measurements).

The dewar has been operating continuously since July 1993 and has demonstrated excellent cryogenic performance. It consistently records a liquid helium boil off of

0.7 litres per hour (120 litres per week), and the nitrogen shield and associated diffusion pump cold traps consume 500 litres of liquid nitrogen per week.

3. Vibration Isolation

The vibration isolation system for the niobium bar is a multistage low pass filter consisting of ten stages at room temperature and a further seven cryogenic stages. Previous theoretical modelling of this systems indicates we achieve ~ 300 dB of isolation (Blair *et al.* 1992).

We are primarily concerned with isolating the fundamental longitudinal mode of the bar. However, the antenna is not a simple one dimensional resonator, and the finite Poisson ratio of the niobium bar implies that longitudinal motion induces a significant radial 'breathing' motion at the waist of the bar. The vibration isolation and suspension system must therefore attenuate both vertical and horizontal vibrations.

The room temperature vibration isolation stack is situated in the central tower and consists of alternating layers of lead masses and rubber springs. The seven stages of all-metal cryogenic isolation are supported by a 500 kg steel intermediate mass which hangs from the room temperature isolation stack by the titanium alloy suspension rod. The cryogenic isolation stages consist of four 13 kg steel masses suspended by short pendula from vertical cantilever springs. The lead/rubber room temperature section and the cryogenic stages attached to the large intermediate mass provide isolation in all six degrees of freedom. The second last isolation stage consists of aluminium cantilevers mounted on a 50 kg steel mass. This gives good vertical isolation, but weaker transverse isolation.

The antenna ultimately rests on a pure titanium 'Catherine wheel', a spiral tapered spring which is soft in all degrees of freedom. It is designed to have internal resonances well above the antenna frequency, a low mass, a high acoustic Q -factor, and a high pressure contact coupling to the bar. The contact points to the bar are defined by annealed copper spacers 10 mm in diameter and 1 mm thick. These are intended to avoid any non-linearity in the contact point, which might cause upconversion of low frequency acoustic noise.

Finite element modelling was used to ensure that none of the suspension components had internal mode frequencies near the antenna normal mode frequencies and their related harmonic mode frequencies. The fundamental flexure mode of the intermediate mass occurs at 790 Hz and is the lowest internal mode in the suspension above the antenna normal mode frequencies. The highest suspension mode below the antenna normal modes is the first mode in the cantilever springs, and this occurs at 350 Hz.

4. Superconducting Microwave Parametric Transducer Readout

Fig. 2 shows a simplified diagram of the antenna and readout system. It operates at about 5 K, and consists of a 1.5 tonne Nb bar with a fundamental frequency of 710 Hz bonded to a 0.45 kg Nb bending flap with a resonant frequency of 700 Hz. The observed coupled frequencies are at 713 Hz (bar-like mode) and 694 Hz (flap-like mode). The bending flap acts as a mechanical amplifier impedance transformer to match the antenna impedance to the mechanical impedance of the transducer (Paik 1974).

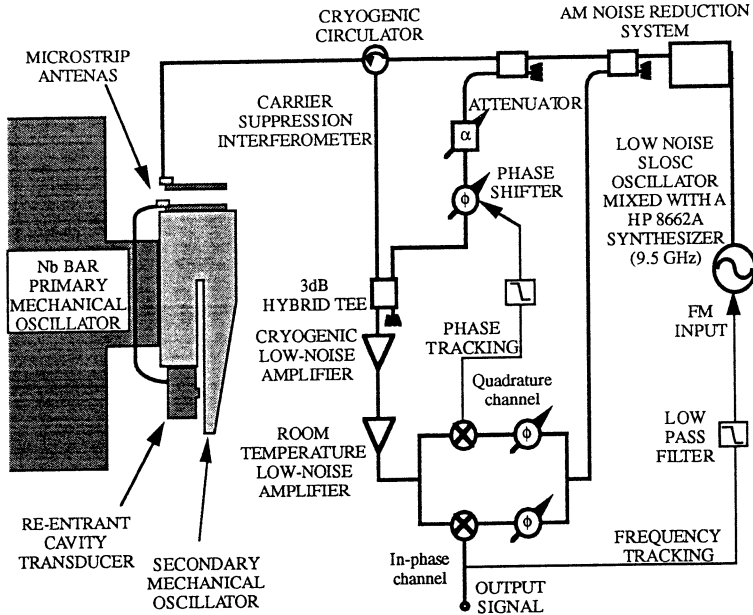


Fig. 2. Diagram of the antenna and transducer system. The carrier suppression interferometer and the microwave amplifier are located in the cryogenic environment. The frequency and phase tracking servos are shown schematically. The re-entrant cavity transducer is pumped by a low noise tuneable microwave source based on a SLOC oscillator.

The vibrational state of the bending flap is continuously monitored by a superconducting re-entrant cavity whose capacitance is modulated by the relative motion of the bar and the bending flap. The low-noise microwave pump signal based on a SLOC oscillator (Giles *et al.* 1989; Tobar and Blair 1994) is coupled radiatively to the transducer by two miniature microstrip antennas (Ivanov *et al.* 1993a). These eliminate the need for any wiring connection between the transducer and its associated electronics, allowing a high level of mechanical isolation of the antenna from the environment. The signal from the transducer is processed in a phase sensitive microwave signal processing circuit (MSPC), comprising an active carrier suppression interferometer, a cryogenic amplifier, and a room temperature mixer. The carrier suppression interferometer is a key element of the MSPC which allows low-noise cryogenic amplification of the extremely weak signal reflected from the transducer. Two servo-control systems provide stable operation of the MSPC. The first servo maintains a constant negative offset between the pump source and transducer resonant frequency. This is required to maintain parametric cold damping, and it also suppresses variations of the transducer resonant frequency caused by low frequency seismic excitation of the normal modes in the vibration isolation system. The second servo maintains the carrier suppression interferometer locked to the 'dark fringe' despite the low frequency rocking motions of the bar, which causes path length variations in the non-contacting coupling.

The interaction of the parametric transducer with the resonant bar causes changes in the resonant frequency and in the Q -factor of the antenna normal

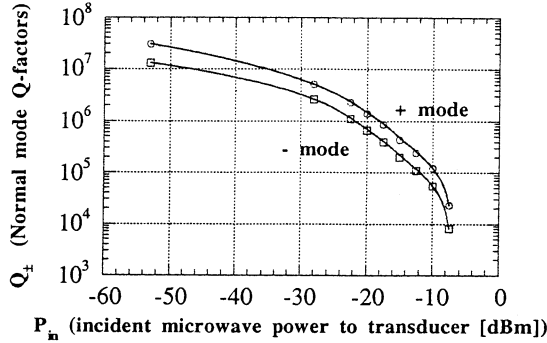


Fig. 3. Measured dependence of the acoustic quality factor on the input power to the transducer, showing the parametric cold damping at high power levels.

modes (Tobar and Blair 1993; Tobar *et al.* 1991; Linthorne *et al.* 1990). These parametric effects can be used to characterise a detector, as shown in the following section. We operate our detector in the cold damped regime. Experimental observations of this effect are shown in Fig. 3. It is shown later that the damping of the oscillator has no detrimental effect on the sensitivity of the detector. The unperturbed Q -factors measured at a very low transducer input power are 3×10^7 and 1.3×10^7 for the bar-like mode (713 Hz) and the flap-like mode (694 Hz) respectively. As the microwave power is increased, non-dissipative parametric cold damping causes the Q -factor to reduce.

5. Characterisation and Calibration of the UWA Detector

To calibrate and characterise the UWA detector we use a two-mode model of a resonant-mass gravitational wave detector interacting with a resonant parametric transducer (Tobar and Blair 1993; Tobar *et al.* 1991; Linthorne *et al.* 1990). A schematic of this model is shown in Fig. 4.

If the pump oscillator frequency varies with respect to the transducer resonant frequency, the pump acts to change the spring constant of the secondary mass. From this effect the detector can be completely characterised and calibrated with respect to this model. Fig. 5 shows how the pump oscillator affects the normal mode frequencies of both the upper (713 Hz) and lower (694 Hz) normal modes (normal mode parameters are represented with + and - subscripts respectively).

From the parametric effects on the resonant frequency shown in Fig. 5, and the measured normal mode parameters presented in Table 1, we can determine the uncoupled mode parameters from the model. These are presented in Table 2.

The current values for the 1993/94 experimental run are consistent with the 1991 experiment. Between these experiments the bending flap was etched to tune it closer to the bar frequency. For perfect tuning the ratio of the electromechanical couplings of the two normal modes, $\beta_r = \beta_+/\beta_-$, is approximately one. Because $m_2/m_1 \ll 1$, the normal mode electromechanical couplings will be dominated by the secondary mass coupling (β_2) (Tobar and Blair 1993). When this is true and $\beta_r = 1$, then $\beta_+ \sim \beta_- \sim \beta_2/2$. The general form of the normal mode couplings

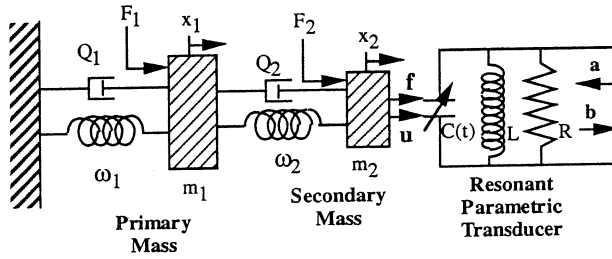


Fig. 4. Schematic of a two-mode resonant-mass GW detector with resonant parametric transducer. The resonant-bar (primary mass) and bending flap (secondary mass) are modelled as two series lumped masses. The displacement of the secondary mass capacitively modulates a resonant parametric transducer. For the UWA GW detector this is a superconducting re-entrant cavity. The two normal modes sensed by the transducer are coupled modes containing a combination of the two uncoupled modes.

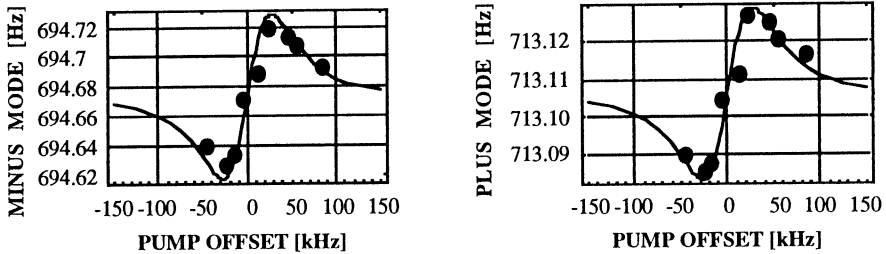


Fig. 5. Normal mode acoustic frequencies as a function of pump oscillator offset from the transducer resonant frequency. The bold line is a theoretical curve while the points are experimental measurements, the uncertainty in measurements being approximately the size of the points.

Table 1. Measured normal mode frequencies and Q -factors, and re-entrant cavity transducer frequency of the UWA GW detector

The measured Nb parameters without the secondary mass attached are also given

Measured parameters	1991	1993/94
$\omega_+/2\pi$ (Hz)	711.334	713.106
$\omega_-/2\pi$ (Hz)	688.859	694.673
$Q_+(\times 10^7)$	1.6 ± 0.05	3.0 ± 0.05
$Q_-(\times 10^7)$	0.37 ± 0.01	1.4 ± 0.05
$\Omega_0/2\pi$ (GHz)	9.7732	9.5
Q_1		$(2.3 \pm 0.3) \times 10^8$
$\omega_1/2\pi$ (Hz)		709.7
m_1 (kg)		755

Table 2. Calculated parameters of the UWA GW detector from the two-mode model and the measured parameters given in Table 1

The discrepancy between the calculated (707.7 Hz) and measured bar frequency (709.7 Hz) is due to mass loading of the bar by the bending flap base

Calculated parameters	1991	1993/94
$\omega_1/2\pi$ (Hz)	707.5	707.7
$\omega_2/2\pi$ (Hz)	692.6	699.9
$Q_1(\times 10^7)$	20 ± 1	20 ± 0.5
$Q_2(\times 10^7)$	0.31 ± 0.01	1.0 ± 0.05
m_2 (kg)	0.45	0.43
β_r	0.213	0.413

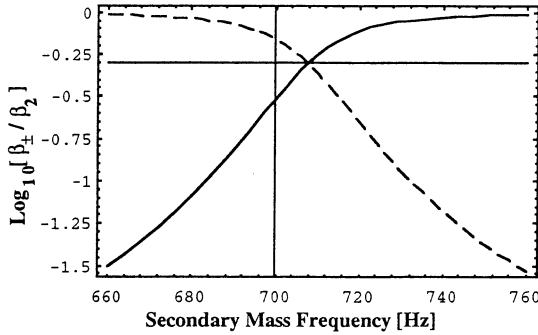


Fig. 6. Normalised mode couplings as a function of secondary mass frequency. The curve represents the + mode and the dashed curve represents the - mode. The vertical line shows the tuning of the bending flap and intersects the normal mode values calculated from the two-mode model. The horizontal line is when $\beta_r = 1$.

has been calculated from the two-mode model previously (Tobar 1995) and is given by

$$\frac{\beta_{\pm}}{\beta_2} = \frac{\partial \omega_{\pm}}{\partial \omega_2} \frac{\omega_2}{\omega_{\pm}}. \quad (1)$$

Fig. 6 shows the dependency of the normalised mode couplings as a function of secondary mass frequency.

To calibrate the antenna we make use of the self-calibrating properties of the re-entrant cavity. The transducer is configured to maximise dv/df ($V \text{ Hz}^{-1}$) at the operating pump offset from resonance. This quantity is measured by frequency sweeping the pump across the transducer resonance and measuring the voltage frequency slope. Thus the displacement sensed by the re-entrant cavity can be calculated from

$$\delta x_{\pm} = (df/dv) (df/dx)^{-1} \delta v_{\pm}. \quad (2)$$

Here δv_{\pm} is the measured voltage response of the normal modes, and df/dx is the displacement sensitivity of the re-entrant cavity transducer ($df/dx \sim 300 \text{ MHz } \mu\text{m}^{-1}$). To first order df/dx is independent of temperature, and can be measured at room temperature. By observing the re-entrant cavity frequency shift from room temperature to 5 K, any second order change in df/dx can then be calculated.

The energy in the normal modes of the oscillator is given by (where k is Boltzmann's constant)

$$E_{\pm} = kT_{\pm}/2 = (m_{\pm} \omega_{\pm}^2 \delta x_{\pm}^2)/2, \tag{3a}$$

and in terms of the normal mode temperatures by

$$T_{\pm} = (m_{\pm} \omega_{\pm}^2 \delta x_{\pm}^2)/k. \tag{3b}$$

Here m_{\pm} are the normal mode masses, which have been shown to be given by (Tobar 1995)

$$\frac{m_{\pm}}{m_2} = \left(\frac{\partial \omega_{\pm}}{\partial \omega_2} \frac{\omega_{\pm}}{\omega_2} \right)^{-1}. \tag{4}$$

Equations (4) are shown as a function of secondary mass frequency in Fig. 7.

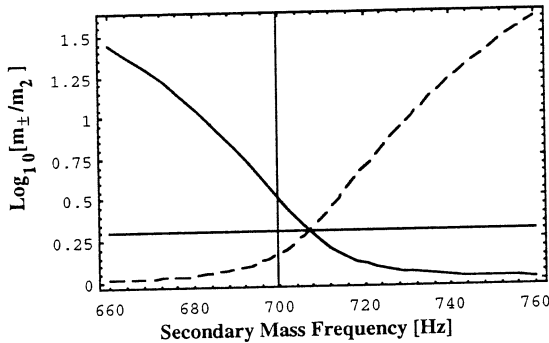


Fig. 7. Normalised normal mode masses as a function of secondary mass frequency. The solid curve represents the + mode and the dashed curve represents the - mode. The vertical line shows the tuning of the bending flap and intersects the normal mode values calculated from the two-mode model. The horizontal line is when $\beta_r = 1$ (i.e. perfectly tuned system), and at this point $m_+ = m_- = 2m_2$.

If the bar and the bending flap were perfectly tuned both modes amplify displacements of the bar by $\sqrt{m_1}/\sqrt{m_2}$, and assuming $m_2 \ll m_1$ both normal mode masses are given by $m_{\pm} = 2m_2$. If the flap is detuned from the bar when $\omega_1 > \omega_2$ the bar becomes an infinite wall with respect to the flap and $m_- \rightarrow m_2, m_+ \rightarrow \infty$; when $\omega_2 > \omega_1$ the flap becomes stiff with respect to the bar and does not act as a displacement amplifier. In this case $m_+ \rightarrow m_2, m_- \rightarrow \infty$.

6. Sensitivity of the UWA Detector

(6a) Experimental Results

The energy of the displacement fluctuations of the resonant-mass system at the frequencies of the normal modes can be expressed in terms of mode temperatures, T_{\pm} . At $P_{\text{in}} = -45$ dBm (input power to re-entrant cavity), T_{\pm} are equal (within experimental error) to the physical temperature of the antenna (about 5 K), consistent with the expected Brownian motion in the antenna. However, the cold damping which reduces the Q -factors also reduces the mode temperature. At low power levels the cold damping preserves the ratio T/Q (Fig. 8), which confirms the intrinsic cold damped operation of the transducer. At higher power levels the ratio T/Q increases proportionally to P_{in}^2 . This occurs due to increased back action noise which arises from pump oscillator amplitude noise which produces fluctuations in the attractive force acting between the transducer and antenna. In the low power regime the antenna sensitivity increases with P_{in} . However, in the back-action regime the sensitivity decreases. Thus the antenna-transducer system is characterised by a classical uncertainty relation for which there is an optimum input power and integration time.

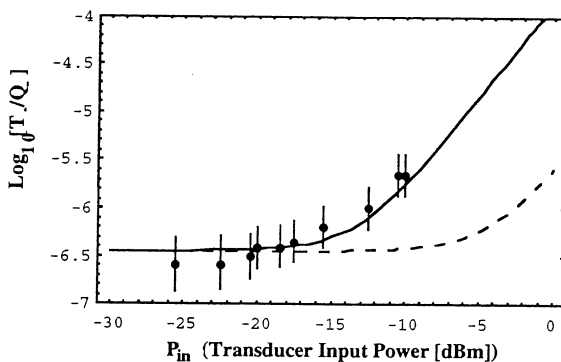


Fig. 8. Dependence of the T/Q ratio of the minus mode on the input power P_{in} to the transducer. The points are experimental measurements and the curves are theoretical calculations. The curves through the points estimate the errors in the T/Q values, while the size of the points estimate the errors in P_{in} . The solid curve represents the T/Q ratio for the present configuration. If the pump amplitude noise is reduced from -140 to -160 dBc/Hz the break point shifts to -3 dBm (dashed curve). The optimum sensitivity occurs at the break point when the input power is -12 dBm. Below -12 dBm the system operates in the non-dissipative cold damped regime where T/Q remains constant. Above -12 dBm the amplitude noise acts back on the oscillator degrading the T/Q ratio proportionally to P_{in}^2 .

For measuring the antenna noise temperature T_n we use a pair of lock-in amplifiers centred on the antenna normal modes, and a zero order prediction (ZOP) algorithm based on this two channel synchronous detection system (Pallottino and Pizzella 1991). When properly tuned this algorithm achieves a signal-to-noise ratio only 2.3 times less than an ideal optimal filter. The noise temperature is determined by fitting the observed energy distribution of the voltage noise at the

filter output to a Boltzmann distribution. The conversion from voltage to energy units is determined in a similar way as the mode temperature described in the last section. An extra factor must be taken into account due to the effect of the ZOP filter (Bonifazi *et al.* 1979). Fig. 9 shows some typical noise temperature values, taken between day 200 and day 235 of 1994. A reproducible exponential behaviour of the normal mode energy distribution was achieved, with a low level of excess high energy events, as shown in Fig. 10.

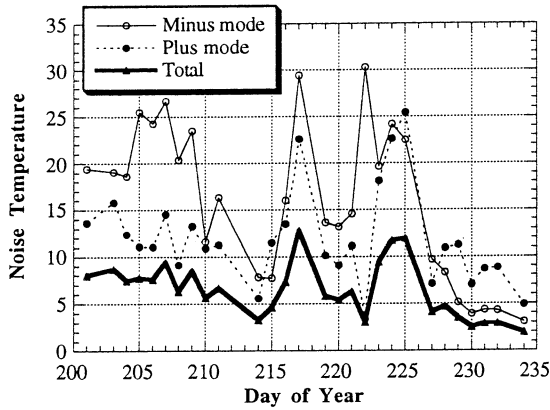


Fig. 9. Noise temperature of the UWA GW detector from day 200 to day 235 of 1994.

Noise temperature versus sampling time for each antenna mode are shown in Fig. 11. A minimum in T_n occurs when contributions from the narrow band noise (Brownian motion and back-action noise) and the broad band noise (additive noise of the readout electronics) are equal. The antenna bandwidth Δf is the reciprocal of the sampling time at which the minimum of T_n is achieved. To calculate the overall noise temperature of the antenna we use the relation $1/T_n = 1/T_{n(713)} + 1/T_{n(694)}$, which comes from the fact that the signal-to-noise ratio is inversely proportional to the noise temperature. This gives a detector noise temperature of 2 mK. Thus with our present scheme we expect the antenna to operate at a noise temperature of about 1 mK when an optimal filter is implemented. This result is consistent with a detailed mathematical model of the detector (Tobar and Blair 1995) presented in Section 6*b*. At the optimum power the broad band noise is 3×10^{-17} m/ $\sqrt{\text{Hz}}$ (referenced to the bending flap). This noise is entirely due to the microwave amplifier. The narrow band noise is 6×10^{-26} N²/Hz for a cold damped mode temperature of 0.5 K.

From Fig. 11 the bandwidth of our antenna is about 1 Hz, which is less than optimum because the bar and flap are detuned by about 10 Hz. This is consistent with our model, which also predicts that more accurate tuning would improve the bandwidth by up to a factor of 3. However detuning affects the strain sensitivity only to second order. Electronic tuning can be achieved by exploiting the parametric interactions of the transducer with the bending flap, but only if the flap mode frequency is above the bar frequency (which is not the present case) (Tobar and Blair 1993). To increase the bandwidth and sensitivity for the existing antenna configuration, both series and back action noise must

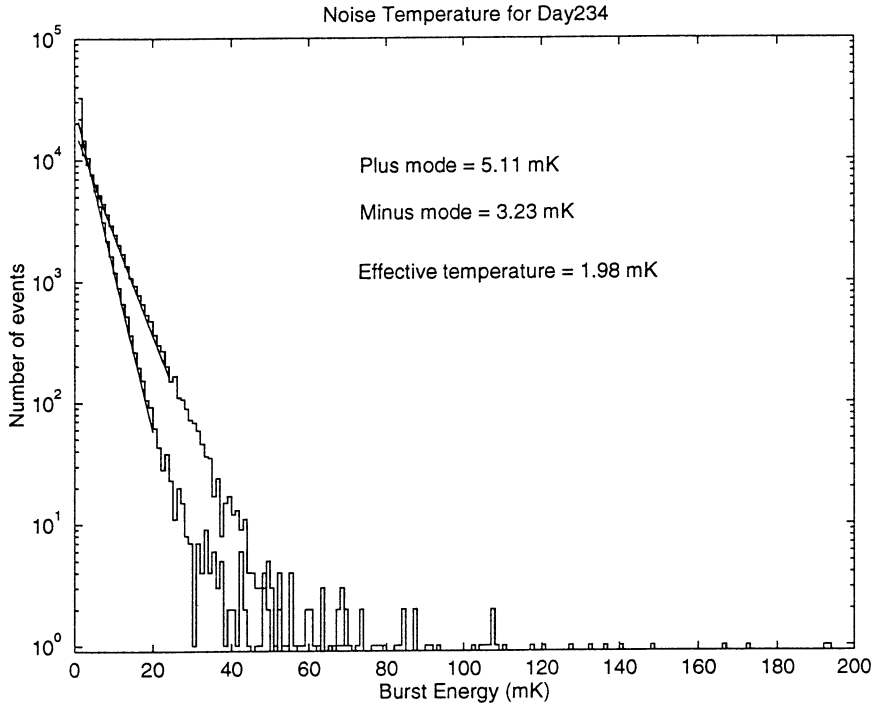


Fig. 10. Effective energy histogram for day 234, 1994, using a ZOP filter. The histograms show expected gaussian behaviour, with about 20 non-Gaussian ‘events’ in the high energy tail.

be reduced. The back action noise is due to amplitude noise in the pump oscillator and the excess series noise is due to the finite carrier signal causing non-linear upconversions in the cryogenic amplifier. A power stabilisation scheme is expected to reduce the a.m. noise from -140 to -160 dBc/Hz (decibels with respect to the carrier per Hz), and the series noise from 5×10^{-17} to 1.5×10^{-18} m/ $\sqrt{\text{Hz}}$. The model shows that for $P_{\text{in}} = -3$ dBm, the noise temperature is reduced to $30 \mu\text{K}$, corresponding to a 1 ms burst strain sensitivity of 10^{-19} with a bandwidth of about 10 Hz. If the bar and the flap were tuned properly the bandwidth would be increased to about 20 Hz. Except for the tuning, these improvements can be implemented without interrupting long term operation.

(6b) Sensitivity Calculation from Noise Spectral Densities

When trying to detect a signal in a noisy environment a standard result in signal detection theory states that the signal-to-noise ratio is optimised by a filter which has a transfer function proportional to the complex conjugate of the signal Fourier transform divided by the total noise spectral density (Wainstein and Zubakov 1962). This principle was first applied to gravitational wave detectors in 1981 (Michelson and Taber 1981), and has become a standard method for determining the performance of resonant-mass gravitational wave detectors (Price 1987; Richard 1986; Bassan 1988; Solomonson *et al.* 1992). To calculate the optimal signal-to-noise ratio we must know all significant noise sources, the

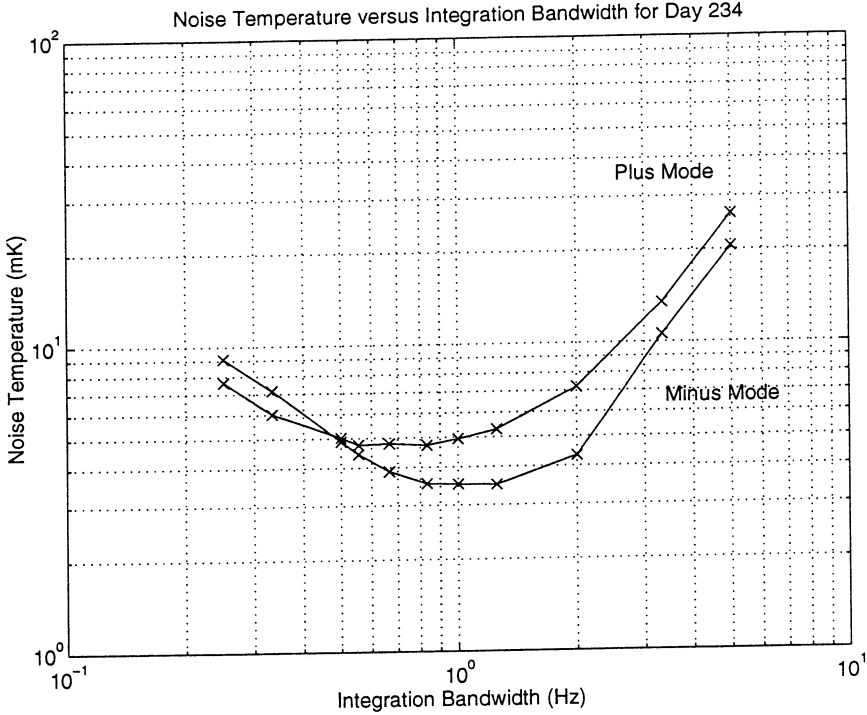


Fig. 11. Noise temperature versus sampling rate for the antenna normal modes.

transfer function of the detector, and the form of the gravitational wave signal. It has been shown that (Michelson and Taber 1981)

$$SNR = \frac{1}{2\pi} \int_{-\infty}^{\infty} \frac{|G_{21}(j\omega)|^2 |F_1(\omega)|^2}{S_{\times 2}(\omega)} d\omega = 4 \int_0^{\infty} \frac{|G_{21}(j2\pi f)|^2 |F_1(f)|^2}{S_{\times 2}^+(f)} df. \quad (5)$$

Here $G_{21}(j\omega)$ is the Fourier transform of the impulse response (or transfer function) of displacement sensed by the transducer per force input at the resonant bar, $F_1(\omega)$ is the Fourier transform of the force input or signal density, and $S_{\times 2}(\omega)$ ($m^2 Hz^{-1}$) is the double-sided spectral density of all noise components referred to a displacement at the transducer. The single-sided spectral density is related to the double-sided spectral density by $S_{\times 2}^+(\omega) = 2S_{\times 2}(\omega)$ (Reif 1965). It is therefore valid to assume that the signal force is an impulse given by $F_1(t) = F_g \delta(t)$ (N), which Fourier transforms to $F_1(f) = F_g = \sqrt{2Em_1}$ ($N Hz^{-1}$), where E is the impulse energy and m_1 is the oscillator effective mass (Michelson and Taber 1981). In a noisy environment the magnitude of the signal density must be compared with the magnitude of the noise density as a function of frequency. Here we define

$$S_n^+(f) = \frac{S_F^+(f)}{\omega m_1}, \quad (6)$$

which has the dimension ($\text{m}\sqrt{\text{Hz}}$), and is a spectral form of the displacement noise referred to a displacement at the resonant bar. Here S_F^+ ($\text{N}/\sqrt{\text{Hz}}$) is the noise referred as an input force spectral density.

Signal strain density and spectral strain sensitivity of a resonant-mass detector. From the calculation of the cross section of a resonant bar antenna to a gravitational burst of suitable polarisation and directivity it has been shown (Pizzella 1975) that the peak displacement at the end of a resonant bar x_{peak} is related to the signal strain density $H_s(f_1)$ (strain/Hz) of the burst by

$$H_s(f_1) = \frac{\pi}{4} \frac{x_{\text{peak}}}{f_1 L}, \quad (7)$$

where L and f_1 are the length and fundamental resonant frequency of the bar respectively. The rms displacement of an oscillator of effective mass m_1 and in equilibrium at temperature T_n is independent of Q and given by

$$\langle x_1 \rangle = \frac{x_{\text{peak}}}{\sqrt{2}} = \sqrt{\frac{kT_n}{m_1 \omega_1^2}}. \quad (8)$$

Thus combining (7) and (8) we obtain

$$H_s(f_1) = \frac{\sqrt{2} \pi}{4 f_1 L} \sqrt{\frac{kT_n}{m_1 \omega_1^2}}, \quad (9)$$

which relates the signal strain density detected with $\text{SNR} = 1$ to the effective noise temperature of the detector. The signal strain density is the natural quantity measured by the detector. To determine the detected strain of the gravitational wave the signal bandwidth must be known (Δf_s), and is approximately given by

$$h = H_s(f_1) \Delta f_s. \quad (10)$$

If the signal bandwidth is greater than the detector bandwidth then Δf_s will not be known and can only be estimated. This will always be true for a gravitational burst. Most gravitational wave groups assume a burst duration of 1 ms, which is equivalent to $\Delta f_s = 1$ kHz.

The resonant bar detector at the University of Western Australia has a large cylindrical niobium bar as the fundamental resonant-mass, with an effective mass of 755 kg (half the bar mass), length of 2.75 m and a fundamental resonant frequency of 710 Hz. Substituting these values in (7) gives $H_s(f_1) = 5.45 \times 10^{-22} \sqrt{T_n(\text{mK})}$ which is equivalent to $h_{1\text{ms}} = 5.45 \times 10^{-19} \sqrt{T_n(\text{mK})}$. The noise temperature can be calculated from (5) by setting $\text{SNR} = 1$ and equating the impulse energy $E = kT_n$. Then by eliminating T_n from (5) and (9) the signal density is calculated to be

$$\frac{1}{H_s(f_1)^2} = 4 \int_0^\infty \frac{1}{h^+(f)^2} df, \quad (11)$$

where

$$h^+(f) = \frac{\pi}{4} \frac{S_n^+(f)}{f L} = \frac{S_F^+(f)}{8 f^2 L m_1}. \quad (12)$$

Note that $h^+(f)$ is related to $S_n^+(f)$ in exactly the same way as $H_s(f_1)$ is related to x_{peak} in (7). This result is consistent with previous results (Price 1987; Dewey 1987). Here $h^+(f)$ is the single-sided rms spectral strain sensitivity (strain/ $\sqrt{\text{Hz}}$) of the resonant bar detector akin to the rms spectral strain sensitivity of an interferometer detector. We can prove this by calculating the optimal detectable strain sensitivity of a resonant bar antenna when the signal bandwidth is less than the detector bandwidth (Δf_d). From (11) it can be shown that

$$h = H_s(f_1) \Delta f_s = \sqrt{\Delta f_s} h^+(f_1)/2. \quad (13)$$

If the detector bandwidth is less than the signal bandwidth, then we obtain

$$h = H_s(f_1) \Delta f_s = \frac{\Delta f_s h^+(f_1)}{2\sqrt{\Delta f_d}}. \quad (14)$$

In general we have

$$h = \frac{\Delta f_s}{2} \left(\int_0^\infty \frac{1}{h^+(f)^2} df \right)^{-\frac{1}{2}}. \quad (15)$$

Equations (13)–(15) give a means of converting from spectral strain sensitivity to strain sensitivity.

Effective bandwidth. To estimate the effective detector bandwidth the signal-to-noise ratio may be written as

$$\text{SNR} = \int_0^\infty \text{Snr}(f) df \approx \text{Snr}(f_0) \Delta f_{\text{eff}}, \quad (16)$$

where $\text{Snr}(f)$ is the signal-to-noise ratio density. The maximum value of Snr occurs at f_0 , and is denoted $\text{Snr}(f_0)$. Thus the effective bandwidth is given by

$$\Delta f_{\text{eff}} \approx \frac{\text{SNR}}{\text{Snr}(f_0)} = h^+(f_0)^2 \int_0^\infty \frac{1}{h^+(f)^2} df = \frac{h^+(f_0)^2}{4H_s(f_0)^2}. \quad (17)$$

From any signal-to-noise ratio or spectral strain density plot for any gravitational wave detector, equation (17) determines an easy method for calculating the detector's effective bandwidth.

Calculation of the UWA detector burst sensitivity. The UWA detector has been operating with a low noise temperature since August 1993 (Blair *et al.* 1995). From the measured noise sources and the known transfer function we can plot the spectral strain sensitivity of the current configuration, shown in Fig. 12. With further anticipated improvements we may be able to reduce the spectral

strain sensitivity as shown in Fig. 12 (Tobar and Blair 1995). Because of excess transducer series noise the sensitivity of our detector is centred around two narrow band regimes corresponding to the two normal modes of the resonant-mass detector. For this configuration the modes can be considered as two separate detectors, with $f_- = 694$ Hz and $f_+ = 713$ Hz, and independent signal-to-noise ratios or noise temperatures. However, when a burst signal is measured both modes will detect a signal, and the net sensitivity will be better than the individual mode sensitivities as given by (19).

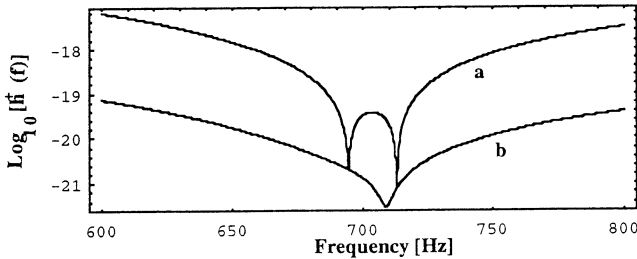


Fig. 12. (a) Current calculated spectral strain sensitivity of the UWA GW detector. (b) Predicted strain sensitivity after major detector improvements.

To calculate the mode temperature from the spectral strain sensitivity we combine equations (5) and (12) to obtain

$$T_n \approx \frac{8 m_1 f_1^4 L^2}{k} \left(\int_0^\infty \frac{1}{h^+(f)^2} df \right)^{-1}. \quad (18)$$

Thus by integrating over each mode separately we calculate T_{n+} and T_{n-} to be 1.6 and 4.4 mK respectively. The values of $h^+(f_+)$ and $h^+(f_-)$ are 7.6×10^{-22} per $\sqrt{\text{Hz}}$ and 2.6×10^{-21} per $\sqrt{\text{Hz}}$ respectively. From (17) the bandwidths of the modes are calculated to be $\Delta f_+ = 0.3$ Hz and $\Delta f_- = 0.8$ Hz. These values are consistent with the measurements using a first order predictor method presented before. To calculate the burst strain sensitivity $h_{1\text{ms}}$ we assume that the gravity wave signal has a 1 kHz bandwidth, and from (14) we calculate $h_{1\text{ms}+} = 6.9 \times 10^{-19}$ and $h_{1\text{ms}-} = 1.1 \times 10^{-18}$. These values are consistent with $h_{1\text{ms}} = 5.45 \times 10^{-19} \sqrt{T_n(\text{mK})}$ as expected. Now to calculate the overall noise temperature or strain sensitivity we must use the following:

$$1/T_n = 1/T_{n+} + 1/T_{n-}, \quad 1/h_{1\text{ms}}^2 = 1/h_{1\text{ms}+}^2 + 1/h_{1\text{ms}-}^2. \quad (19)$$

Thus the overall detector sensitivity is $T_n = 1.2$ mK and $h_{1\text{ms}} = 5.9 \times 10^{-19}$.

With major improvements to the parametric transducer it seems possible that curve b in Fig. 12 may be achieved (Tobar and Blair 1995). In this configuration the series noise would be low enough that the sensitivity would be largest between the two modes, and occur at $f_0 = 708.8$ Hz with $h^+(f_0) = 3.3 \times 10^{-22}$ per $\sqrt{\text{Hz}}$. From (18) and (14) the sensitivity of this configuration is $T_n = 13$ μK and $h_{1\text{ms}} = 6.3 \times 10^{-20}$, with a 6 Hz bandwidth.

7. Sensitivity to Monochromatic Signals

Recently the millisecond pulsar (PSR0437-4715) was discovered (Johnson *et al* 1993) and shown to be just 100 parsecs away. It is fortuitous that the fourth harmonic of its frequency (694.75 Hz) is exactly the same (to within the bandwidth of 1 Hz) as the minus mode of the UWA gravitational wave antenna. From Fig. 12 and equation (11), the calculated sensitivity for an observation with the UWA detector is $h = 5 \times 10^{-25}$ after $\tau = 1000$ hours integration (here we substitute $\Delta f_s = 1/\tau$). So far about 40 millisecond pulsars have been discovered and, as the bandwidth of resonant-mass GW detectors increases with improved technology, so will the probability of monochromatic wave detection.

8. Data Acquisition and Analysis

The data acquisition and processing system for the microwave signal is shown schematically in Fig. 13. The output of the mixer is amplified, bandpass filtered, and then phase sensitively detected with two 'lock-in' amplifiers tuned to the resonant frequencies of the antenna normal modes. The data acquisition software is installed on a Macintosh Iix personal computer equipped with a 12-bit A/D converter. The two quadratures outputs of each lock-in are sampled at 10 Hz, recorded to hard disk, and automatically transferred to a SUN workstation for data processing. The raw data are archived periodically to an 8 mm Exabyte tape, copies of which are stored off-campus. Each block of recorded data contains the timing of its first record, from which the times of all the other samples in the block may be determined. Timing information to an accuracy of ± 1 ms is provided by a cesium clock at CSIRO which is accessed via a computer network. This may be replaced by timing from the Global Positioning System should the network time prove unreliable.

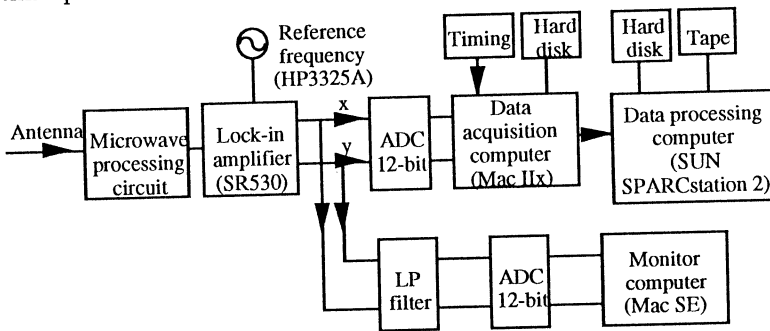


Fig. 13. Block diagram of the data acquisition system.

The data processing and display software is written in MATLAB, and is based on software developed by the research group at Louisiana State University for their Allegro antenna. The recorded data are filtered with a two-pole lowpass filter (at an appropriate cutoff frequency) so as to reduce the effects of aliasing, before being resampled at the optimum sampling rate. Presently, the noise temperatures of the antenna normal modes are calculated using a zero order prediction (ZOP) algorithm as discussed previously in Section 6.

A continuously updated record of the antenna performance is generated and stored. Noise temperature histograms are generated hourly and placed in an

antenna performance summary file. All calculations are performed at the previously determined optimum sampling rate. The impulsive events with energies above a certain threshold are catalogued, to form a daily list of candidate gravitational wave events to be exchanged with researchers operating other detectors. These events are first vetoed against electromagnetic pulse, cosmic ray, and seismic monitors located near the antenna.

Continuous real-time data monitoring and analysis of the two antenna modes is also performed by two Macintosh SE personal computers equipped with a 12-bit A/D converter. The two quadratures outputs of the lock-ins are low pass filtered and then sampled at 1 Hz. The computers calculate and display the instantaneous vibration energies of the antenna modes, and the cumulative mode temperature and noise temperature histograms. This information is used for diagnostic purposes.

9. Conclusions

The gravitational wave antenna at the University of Western Australia has achieved a noise temperature of less than 2 mK. This vindicates our alternative antenna design strategy based on a high Q -factor niobium bar, four-point antenna suspension, and a superconducting parametric transducer. Minor improvements to the transducer and data processing should reduce the noise temperature without interrupting the long-term operation of the antenna.

Acknowledgments

Thanks to Arthur Woods, Ron Bowers, John Devlin, Alan Gorham, Richard Meager, John Moore, Derek Newman, and Graham Warburton for their invaluable contributions to our mechanical systems, and to John Cryer for the supply of cryogenic fluids. We would also like to thank the Italian and United States resonant bar groups for their continued support. This work was supported by the Australian Research Council.

References

- Astone, P., *et al.* (1993). *Phys. Rev. D* **47**, 362.
- Bassan, M. (1988). *Phys. Rev. D* **38**, 2327.
- Blair, D. G., *et al.* (1992). Sixth Marcel Grossmann Meeting on Recent Developments in Theoretical and Experimental General Relativity, Gravitation and Relativistic Field Theories (Eds H. Sato and T. Nakamura), p. 1293 (World Scientific: Singapore).
- Blair, D. G., *et al.* (1993). In 'Some New Trends in Fluid Mechanics and Theoretical Physics' (Eds C. C. Lin and N. Hu), p. 591 (Peking University Press: Beijing).
- Blair, D. G., Ivanov, E. N., Tobar, M. E., Turner, P. J., van Kann, F., and Heng, I. S. (1995). *Phys. Rev. Lett.* **74**, 1908.
- Bocko, M. F., and Johnson, W. W. (1984). *Phys. Rev. A* **30**, 2135.
- Bonifazi, P., Ferrari, V., Frasca, S., Pallottino, G. V., and Pizzella, G. (1979). *Nuovo Cimento* p. 3012.
- Braginsky, V. B., and Manukin, A. B. (1977). In 'Measurement of Weak Forces in Physics Experiments', p. 19 (University of Chicago Press).
- Dewey, D. (1987). *Phys. Rev. D* **36**, 6.
- Giles, A. J., Jones, S. K., Blair, D. G., and Buckingham, M. J. (1989). Proc. 43rd Symp. on Frequency Control, p. 89 (IEEE: New Jersey).

- Hamilton, W. O. (1992). Sixth Marcel Grossmann Meeting on Recent Developments in Theoretical and Experimental General Relativity, Gravitation and Relativistic Field Theories (Eds H. Sato and T. Nakamura), p. 988 (World Scientific: Singapore).
- Ivanov, E. N., Tobar, M. E., Turner, P. J., and Blair, D. G. (1993a). *Rev. Sci. Instrum.* **64**, 1905.
- Ivanov, E. N., Turner, P. J., and Blair, D. G. (1993b). *Rev. Sci. Instrum.* **64**, 3191.
- Johnson, S., *et al.* (1993). *Nature* **361**, 613.
- Linthorne, N. P., Veitch, P. J., and Blair, D. G. (1990). *J. Phys. D* **23**, 1.
- Michelson, P. F., and Taber, R. C. (1981). *J. Appl. Phys.* **52**, 4313.
- Paik, H. J. (1974). Ph.D. Thesis, Stanford University.
- Pallottino, G. V., and Pizzella, G. (1991). In 'The Detection of Gravitational Waves' (Ed. D. G. Blair), p. 243 (Cambridge University Press).
- Pizzella, G. (1975). *Riv. Nuovo Cimento* **5**, 369.
- Price, J. C. (1987). *Phys. Rev. D* **36**, 3555.
- Reif, F. (1965). 'Fundamentals of Statistical and Thermal Physics' (McGraw-Hill: New York).
- Richard, J.-P. (1986). *J. Appl. Phys.* **60**, 3807.
- Solomonson, N., Johnson, W. W., and Hamilton, W. O. (1992). *Phys. Rev. D* **46**, 2299.
- Tobar, M. E. (1995). *J. Phys. D* (to be published).
- Tobar, M. E., and Blair, D. G. (1993). *J. Phys. D* **26**, 2276.
- Tobar, M. E., and Blair, D. G. (1994). *IEEE Trans. MTT* **42**, 344.
- Tobar, M. E., and Blair, D. G. (1995). *Rev. Sci. Instrum.* **66**, 2751.
- Tobar, M. E., Linthorne, N. P., and Blair, D. G. (1991). In 'Gravitational Astronomy: Instrument Design and Astrophysical Prospects' (Eds D. E. McClelland and H. A. Bachor), p. 368 (World Scientific: Singapore).
- Turner, P. J., and Blair, D. G. (1992). Sixth Marcel Grossmann Meeting on Recent Developments in Theoretical and Experimental General Relativity, Gravitation and Relativistic Field Theories (Eds H. Sato and T. Nakamura), p. 1529 (World Scientific: Singapore).
- Veitch, P. J., *et al.* (1987). *Rev. Sci. Instrum.* **58**, 1910.
- Wainstein, L. A., and Zubakov, V. D. (1962). 'Extraction of Signals from Noise' (Prentice Hall: Englewood Cliffs, NJ).
- Weber, J. (1960). *Phys. Rev.* **117**, 306.
- Xu, B.-X., Hamilton, W. O., Johnson, W. W., and Solomonson, N. (1989). *Phys. Rev. D* **40**, 1741.

